Nucleation of solid solutions crystallizing from aqueous solutions

By Andrew Putnis[1], Carlos M. Pina[2], Jose M. Astilleros[1], Lurdes Fernández-Díaz[2] and Manuel Prieto[3]

[1]*Institut für Mineralogie, University of Münster, Corrensstrasse 24, 48149 Münster, Germany*
[2]*Departamento de Cristalografía y Mineralogía, Universidad Complutense de Madrid, 28040 Madrid, Spain*
[3]*Departamento de Geología, Universidad de Oviedo, 33005 Oviedo, Spain*

The study of nucleation and growth mechanisms of salts from aqueous solutions, as a function of supersaturation, is described using both macroscopic and microscopic experiments. *In situ* observations in a fluid cell in an atomic force microscope (AFM) reveal phenomena not accounted for in standard crystal-growth theories, specifically on the role of the crystal structure of the substrate in controlling spiral growth and two-dimensional nucleation. As a model example, the crystallization of two isostructural salts, $BaSO_4$ and $SrSO_4$, is described. The growth of solid-solution crystals is considerably more complex. The supersaturation of a given aqueous solution relative to a solid solution is different with respect to each solid composition, and it leads to the possibility that different compositions can simultaneously grow by different mechanisms on the same crystal face. Oscillatory compositional zoning is another consequence of the interplay between the thermodynamics and the kinetics of nucleation. The factors which control nucleation and growth of the solid solution $(Ba,Sr)SO_4$ from an aqueous solution are described. The predictions made from the theory are compared with direct observations of crystal growth in an AFM.

Keywords: solid solutions; crystallization; two-dimensional nucleation; spiral growth; atomic force microscopy

1. Introduction

The crystallization of salts from aqueous solutions has been the subject of research for many years, and the fundamental ideas are generally well understood (e.g. Mullin 1993). However, crystal growth is a complex process involving bulk diffusion through the fluid, surface adsorption and diffusion and finally the integration of ions/molecules into the crystal lattice (Nielsen 1984; Nielsen & Toft 1984; Chernov 1984; Sunagawa 1993; Sarig 1993), and ultimately these processes depend on the reactivity of the crystal surface as well as the saturation state of the fluid. Crystal-growth mechanisms such as spiral growth, two-dimensional nucleation and continuous growth have been inferred from experimental data on macroscopic growth

rates as a function of increasing fluid supersaturation (Sunagawa 1984, 1987, 1993), although understanding the critical supersaturation values for each mechanism is complicated by many factors that can influence the actual supersaturation at which nucleation occurs.

The integration of molecules occurs preferentially at kink sites which occur along atomic steps on a crystal surface, and so the generation of new monomolecular steps is important for understanding the overall crystal-growth rate. With *in situ* crystal-growth experiments in an atomic force microscope (AFM), it has been possible to verify the classical models of crystal growth in which monolayer steps on a crystal surface are generated either by the presence of screw dislocations, resulting in spiral growth (Burton *et al.* (1951) (BCF) model), or by the formation of new islands on a flat surface (two-dimensional nucleation, or the 'birth and spread' model (Ohara & Reid 1973)). It is generally assumed that bulk crystal-growth rate is controlled by spiral growth at low supersaturations and by surface nucleation at higher supersaturations (Sunagawa 1993). This paper investigates these two mechanisms in relation to supersaturation and surface crystal structure, using two isostructural salts, barite, $BaSO_4$, and celestite, $SrSO_4$, as model examples.

These two simple salt compositions are end-members of a solid solution. The growth of solid solutions from multicomponent aqueous solutions is more complex than that of pure end-members and is poorly understood. Only relatively recently have there been significant advances in understanding the thermodynamics of such solid-solution–aqueous-solution (SS–AS) systems (Lippmann 1980, 1982; Glynn & Reardon 1990). The way in which the supersaturation of a given aqueous solution should be defined, relative to all possible solid-solution compositions, is still controversial (Prieto *et al.* 1993; Pina *et al.* 2000; Astilleros *et al.* 2002). For the thermodynamic representation of SS–AS systems, the mixing properties of the solid solution as well as the aqueous solution must be known. From the experimental point of view, it is also difficult to separate thermodynamic and kinetic effects in crystal-growth experiments.

In this paper we use the model example of the nucleation and growth of $(Ba,Sr)SO_4$ from aqueous solution. The solid solution is assumed to be approximately ideal (i.e. very small enthalpy of mixing), but the solubility products of the two end-members differ by three orders of magnitude. Although the degree of ideality of the $(Ba,Sr)SO_4$ solid solution has been widely discussed (e.g. Becker *et al.* 2000), the main controlling factor of its nucleation and growth behaviour is the large difference in solubility of the end-members. Such a situation is not unusual and has important implications. In natural systems (i.e. minerals), the crystallization of solid solutions from aqueous solutions is the norm, and our ultimate aim here is to understand factors underlying crystal-growth phenomena common in solid solutions, such as compositional oscillatory zoning.

2. Experiment

The observations and results come from two different types of crystallization experiments. In the first, crystallization takes place by the counter-diffusion of reactants through a column of porous silica hydrogel. In such an experiment, nucleation is suppressed and takes place at relatively high supersaturation (Henisch 1989). The experimental arrangement is shown in figure 1. For the growth of $BaSO_4$, $SrSO_4$ and

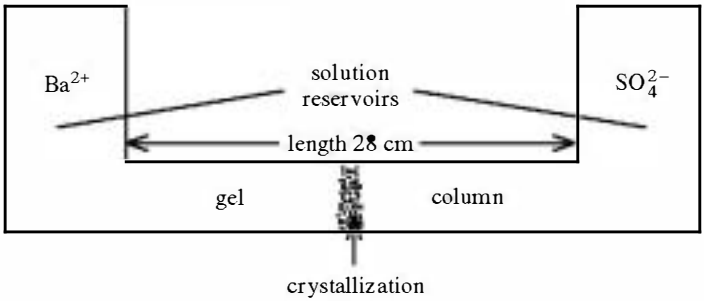

Figure 1. Schematic of the experimental arrangement for crystal growth by counter-diffusion through a microporous silica hydrogel column.

the (Ba,Sr)SO_4 solid solution, the Ba^{2+} and Sr^{2+} ions are contained in a reservoir on one side of the hydrogel column, and the SO_4^{2-} ions are contained on the other. Counter-diffusion results in eventual crystallization near the centre of the column. The time dependence of the concentration gradients of each species as a function of starting concentration in the reservoirs has been predetermined. The supersaturations are determined from a Debye–Huckel calculation of the activities of all components. Thus, nucleation takes place under controlled conditions of supersaturation and *supersaturation rate* (Prieto *et al.* 1990, 1991, 1994). This second factor is very important and is discussed further below.

In the second type of experiment, nucleation and growth were studied directly in the fluid cell of an AFM, on a substrate of either $BaSO_4$ or $SrSO_4$. Fluids of varying supersaturations were passed over the substrate and processes such as step advancement, spiral growth and two-dimensional nucleation observed. The experimental details can be found in Bosbach *et al.* (1998), Pina *et al.* (2000) and Risthaus *et al.* (2001).

3. Crystal growth of the pure end-members $BaSO_4$ and $SrSO_4$

(*a*) *Macroscopic growth experiments*

The principal result from experiments involving the counter-diffusion of species through an inert hydrogel transport medium is that the supersaturation at which nucleation takes place is highly dependent on the starting conditions, i.e. the initial concentration of the reactants in the reservoirs. The higher the concentrations in the reservoirs, the faster the rate of change of supersaturation throughout the column, and the higher the value of the supersaturation at which nucleation occurs. This value of supersaturation may be termed the *threshold supersaturation* and is a kinetic concept, determined by the rate of departure from equilibrium (the supersaturation rate). It is thus different from the concept of a *critical supersaturation*, which is essentially a thermodynamic concept dependent on the positive and negative energy terms associated with the formation of a critical nucleus (as in classical nucleation theory). Before outlining the experimental results, it is convenient to review these concepts of critical and threshold supersaturation.

In classical homogeneous nucleation theory, the theoretical nucleation rate, J, i.e. the number of nuclei formed per unit volume and time, is given by (Nielsen 1964)

$$J = \Gamma \exp\left(\frac{-\delta\sigma^3\Omega^2}{k^3T^3(\ln S)^2}\right), \tag{3.1}$$

where δ is a shape factor, σ is the nucleus–solution interfacial tension and Ω is the volume of one growth unit in the nucleus. The pre-exponential factor Γ, described in more detail below, is related to the rate at which the nucleus can grow to a supercritical size, and hence it involves volume diffusion. T is the temperature and k is Boltzmann's constant. S is the supersaturation ratio C/C_s, where C_s is the concentration of the solution in equilibrium with the crystalline phase and C is the actual concentration of the solution. From equation (3.1) the nucleation rate is a very sharp function of supersaturation. It is usual to define the critical supersaturation as that corresponding to a nucleation rate of 1 nucleus s^{-1} cm^{-3}.

Another important concept in the classical theory is the relationship between the solubility and the critical supersaturation. First, the interfacial tension σ is related inversely to the solubility, so that the higher the solubility, the lower the surface tension and the lower the critical supersaturation (Söhnel 1982; Mullin 1993). Second, the pre-exponential factor Γ in equation (3.1) also increases with solubility. This can be seen by evaluating Γ (Walton 1967, 1969) as

$$\Gamma = \nu_0 N_0 A^* \exp\left(\frac{\Delta G_v}{kT}\right), \tag{3.2}$$

where ν_0 is a frequency factor, A^* is the surface area of the critical nucleus and ΔG_v is the activation energy barrier for diffusion from the bulk solution to the growing nucleus. N_0 is the number of growth units per unit volume of solution. In this context 'growth units' may be the molecules or ions which cluster to form the crystalline phase. In solutions of sparingly soluble substances N_0 is small and the growth units are relatively distant from one another.

The classical concepts above assume that supersaturation is uniform throughout the system. The concept of a supersaturation gradient cannot readily be accommodated into such a formulation. The critical supersaturation has no meaning in a situation where the supersaturation changes rapidly and metastable states are preserved. The maximum supersaturation or the metastability limit which can be achieved under any given set of conditions is a kinetic concept—the threshold supersaturation. As in all kinetic concepts, the value of the threshold supersaturation will depend not only on the nature of the solute and solvent, but also on the temperature, stirring and the fluid dynamics of the solution, its thermal history, the total mass of the solution, etc. (Khamskii 1969). In any experimental determination of supersaturation it is the threshold value which is determined, unless the assumptions of the classical theory can be shown to apply. The threshold supersaturation is the relevant concept whenever supersaturation gradients exist. Similarly, the time taken to form nuclei depends on supersaturation gradients. This 'waiting time' is therefore different from the 'incubation time' for nucleation, which is a concept related to crystallization under uniform conditions.

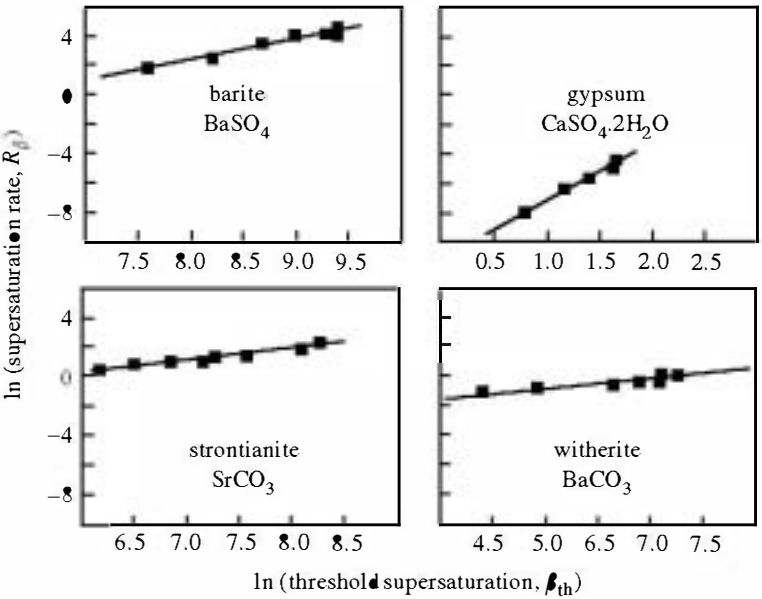

Figure 2. The correlation between the threshold supersaturation $\beta_{\rm th}$ and the supersaturation rate R_β as a linear plot of $\ln \beta_{\rm th}$ against $\ln R_\beta$.

(*b*) *Experimental results*

In all cases studied (Putnis *et al.* 1995) there is an empirical relationship between the supersaturation rate, R_β, and the threshold supersaturation $\beta_{\rm th}$ given by

$$R_\beta = K(\beta_{\rm th})^m, \tag{3.3}$$

where K and m are empirical coefficients (figure 2). The relationship between threshold supersaturation and supersaturation rate applies to a range of substances with widely differing solubilities as well as to $BaSO_4$ supersaturated to a very high degree by inhibitors, suggesting that the values of the empirical parameters K and m describe some fundamental aspects of the nucleation process. However, there is no obvious correlation between solubility or interfacial tension and either m or K. Mullin (1993) concluded that the exponent m has no fundamental significance, contrary to earlier suggestions relating it to the number of elementary species involved in the nucleation process.

Equation (3.3) also applies in cases where the rate of change of supersaturation is due to cooling rather than diffusion control. Nývlt (1968) measured the ΔT, to crystallize various salt solutions, as a function of the cooling rate b. For an undercooling ΔT, the supersaturation was defined as the maximum absolute supersaturation $\Delta C_{\rm max} = C - C_{\rm s}$, where $C_{\rm s}$ is the equilibrium concentration of the salt at crystallization temperature and C is the actual concentration used. The temperature dependence of the equilibrium concentration is given by $dC_{\rm s}/dT$. Nývlt found that for aqueous solutions of more than 25 substances the data could be fitted to the equation

$$\frac{dC_{\rm s}}{dT} b = K(\Delta C_{\rm max})^n. \tag{3.4}$$

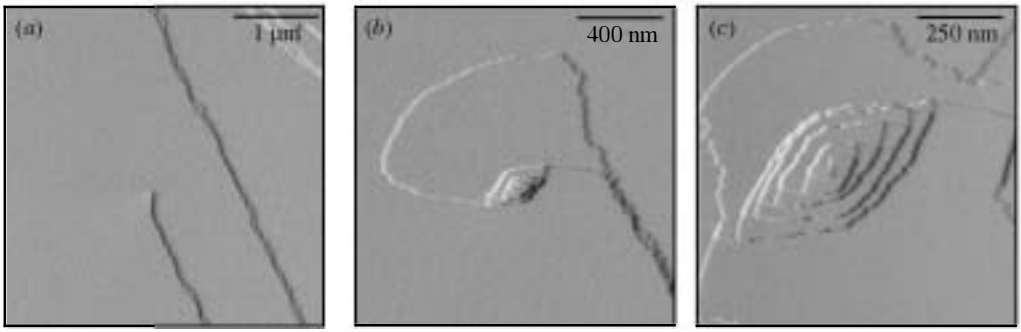

Figure 3. (*a*) AFM image of an (001) cleavage surface of barite showing cleavage steps, one of which terminates at a screw dislocation core. Deionized water that is passed through the fluid cell slightly dissolves the step edges, separating the two $BaSO_4$ layers in each step. (*b*) With the introduction of a slightly supersaturated $BaSO_4$ solution, a growth step one $BaSO_4$ layer thick migrates from the site of the dislocation core but growth is highly anisotropic and restricts the development of the spiral. (*c*) Detail of the spiral which is made up of two interpenetrating spirals made of alternate $BaSO_4$ layers.

It is clear that R_β in equation (3.3) controls β_{th} in the same way that b controls $\Delta C_{\max}$ in equation (3.4).

The values of threshold supersaturation for $BaSO_4$ and $SrSO_4$ reflect the large difference in solubility of these salts. The solubilities, expressed as the logarithm of the solubility product at equilibrium, $\log K_{\mathrm{sp}}$, are -9.96 for $BaSO_4$ and -6.62 for $SrSO_4$ (Blount 1977; Reardon & Armstrong 1987). Threshold supersaturation for nucleation under the same experimental conditions is typically two orders of magnitude higher for barite than celestite. For example, for given starting concentrations of the reservoir solutions and a specific experimental design (i.e. diffusion length in the column, porosity of the silica gel, etc.) the threshold supersaturation for barite is 1.2×10^4 compared with 1.3×10^2 for celestite (Prieto *et al.* 1993). These overall high values are due to crystallization in a gel. In a free solution, where mass transport can take place by convection, such large departures from equilibrium are not achievable. This is addressed in the next set of experiments. The large difference in threshold supersaturation has important implications when considering the crystallization of SS–AS systems.

4. Crystal-growth experiments in a fluid cell in an AFM

Both $BaSO_4$ and $SrSO_4$ crystals have perfect cleavage on (001) and flat faces can be easily prepared as substrates for *in situ* crystal-growth experiments. Aqueous solutions with known supersaturation were used to determine the range of supersaturations where crystal growth takes place by step advancement, and the critical value at which two-dimensional nucleation occurs. These cleaved surfaces have many cleavage steps, as well as points of intersection with screw dislocation lines providing step edges and sites for spiral growth. Figure 3 shows a crystal-growth sequence where a fluid containing Ba^{2+} and SO_4^{2-} ions at a supersaturation value of 12 is passed over a barite (001) cleavage surface (Pina *et al.* 1998*a*, *b*). To interpret such images it is important to note that the unit cell of barite consists of two $BaSO_4$

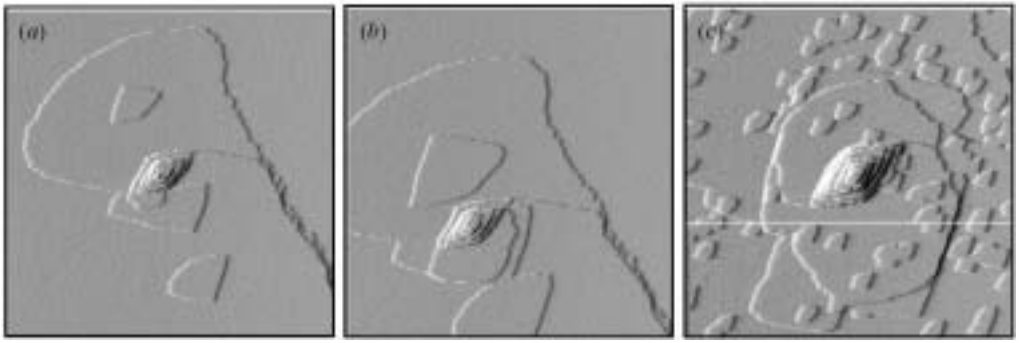

Figure 4. (*a*) AFM image of an (001) cleavage surface showing *in situ* two-dimensional nucleation. Note the two opposite orientations of the islands on each different $BaSO_4$ substrate layer. Growth normal to the curved step of the island is *ca.* 10 times faster than in the opposite direction. (*b*) The spiral can only spread when underpinned by one of the spreading islands. (*c*) Increasing the supersaturation greatly increases the nucleation rate. The image area in each case is 2 μm × 2 μm.

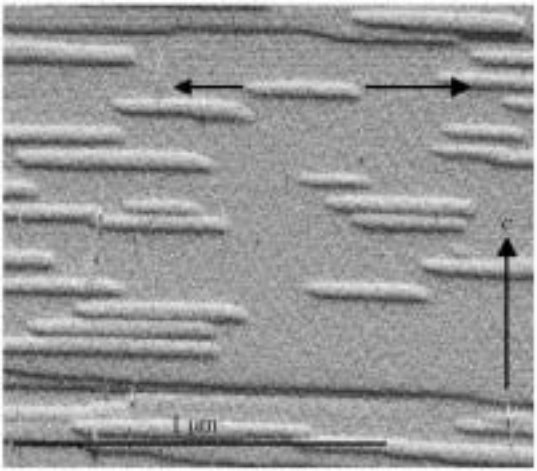

Figure 5. Two-dimensional nucleation on a (210) surface of barite. Islands grow as needles, one $BaSO_4$ layer thick, preferentially along the ⟨120⟩ direction, shown by the longer arrow.

layers parallel to (001), and that each layer is related by a 2_1 screw-axis parallel to the *c*-axis.

In figure 3*a*, deionized water had been passed over the barite surface, which shows two cleavage steps, one terminated at a screw dislocation. Each cleavage step is 7.2 Å high, but is differentiated into two layers by the anisotropic dissolution due to the initial water treatment (to clean the surface). Injection of the $BaSO_4$ solution begins step growth, with new steps being one $BaSO_4$ layer thick (3.6 Å). The cleavage steps migrate normal to their length, and spiral growth begins at the dislocation core. A new $BaSO_4$ layer spreads away from the core to one side but does not continue around the spiral as in classical descriptions of spiral growth (figure 3*b*). Instead, the spiral becomes increasingly tightly wound around the core with very little lateral growth (figure 3*c*), due to the marked anisotropy of the growth rate within such a layer. This becomes obvious when eventually two-dimensional nucleation takes place on the surface, with islands having a sector-shaped morphology (figure 4*a*).

Growth normal to the curved surface is an order of magnitude faster than growth normal to the straight sides of the islands. The islands have a different orientation, related by a 2_1-axis, depending on which of the two possible $BaSO_4$ layers is the substrate. The anisotropy is a structurally induced self-inhibitor for spiral growth. The spiral can only continue to grow if one of the islands provides an underpinning over which the fast-growing layer can grow (figure 4*b*). When the supersaturation of the fluid is increased, the nucleation rate increases significantly (figure 4*c*) and reaches a catastrophic rate as the supersaturation is increased yet further.

Such anisotropy was not envisaged in the theories that suggested that spiral growth was the dominating growth mechanism at low supersaturations. In the case above, spiral growth can only take place together with two-dimensional nucleation, and thus only at a sufficiently high supersaturation. This point is more strongly emphasized when considering nucleation and growth on the (210) surface of barite. The anisotropy in this case is so great that the nuclei are needle-shaped (figure 5), growing predominantly in one direction. Under such circumstances, spiral growth on (210) is not considered a possibility.

From these measurements it is possible to determine the transitional supersaturation values between spiral growth and two-dimensional nucleation. For the growth of pure $BaSO_4$ on a $BaSO_4$ (001) substrate this value is 7.0. For the equivalent case of nucleation of $SrSO_4$ on a (001) celestite surface, it is 2.3 (Pina *et al.* 2000). These values are subject to experimental conditions such as surface topography, fluid flow rate, temperature and the orientation of the face, but for the purposes of the present paper, they are values which will be relevant when considering the growth of $(Ba,Sr)SO_4$ solid solutions.

5. Crystal growth of the $(Ba,Sr)SO_4$ solid solution from aqueous solution

Compared to pre-end-members, growth of a solid solution is much more complex, both in the definition of equilibrium and of supersaturation, and also in the nature of the crystallization process. Before describing relevant observations we briefly review the concepts of equilibrium and supersaturation in SS–AS systems.

(*a*) *Equilibrium in SS–AS systems*

For a pure solid, the solubility product K_{sp} is defined as the product of the activities of the relevant ionic species in solution; e.g. for $BaSO_4$ $K_{sp} = [Ba^{2+}][SO_4^{2-}] = 1.096 \times 10^{-10}$. To describe the solubility of solid solutions the solubility concept must be extended to binary systems. Following Lippmann (1980, 1982) and Glynn & Reardon (1990), the aqueous solubility of a solid solution may be described by the partial solubility products of the end-members. In the case of barite-celestite solid solutions, equilibrium is defined by the mass action equations

$$[Ba^{2+}][SO_4^{2-}] = K_{Ba}a_{Ba}, \qquad [Sr^{2+}][SO_4^{2-}] = K_{Sr}a_{Sr}, \tag{5.1}$$

where $[Ba^{2+}]$, $[Sr^{2+}]$, and $[SO_4^{2-}]$ are the activities of the ions in the aqueous solution, a_{Ba} and a_{Sr} are the activities of the components $BaSO_4$ and $SrSO_4$ in the solid solution, and K_{Ba} and K_{Sr} are the thermodynamic solubility products of the pure end-members.

Lippmann introduced the concept of the 'total solubility product' variable $\Sigma\Pi$, which is defined as the sum of the partial solubility products contributed by the individual end-members of the solid solution. For the present example

$$\Sigma\Pi = [SO_4^{2-}]([Ba^{2+}] + [Sr^{2+}]). \tag{5.2}$$

At thermodynamic equilibrium, combining equations (5.1) and (5.2) yields

$$\Sigma\Pi_{eq} = K_{Ba}a_{Ba} + K_{Sr}a_{Sr} = K_{Ba}X_{Ba}\gamma_{Ba} + K_{Sr}X_{Sr}\gamma_{Sr}, \tag{5.3}$$

where X_{Ba}, X_{Sr} are the mole fractions of the components $BaSO_4$ and $SrSO_4$ in the solid and γ_{Ba}, γ_{Sr} are the solid-phase activity coefficients.

The equilibrium value of the total solubility product $\Sigma\Pi_{eq}$ is termed the 'solidus' and is the value of $\Sigma\Pi$ that defines equilibrium for a given solid-solution composition. To completely describe the equilibrium, a second relation, known as the 'solutus' is used to express $\Sigma\Pi_{eq}$ as a function of the aqueous-solution composition. This is derived from equations (5.1) and (5.2) and substituting the definitions of the aqueous activity fractions, $X_{Ba,aq}$ and $X_{Sr,aq}$,

$$X_{Ba,aq} = \frac{[Ba^{2+}]}{[Ba^{2+}] + [Sr^{2+}]} \tag{5.4}$$

and

$$X_{Sr,aq} = \frac{[Sr^{2+}]}{[Ba^{2+}] + [Sr^{2+}]}. \tag{5.5}$$

The Lippmann solutus equation is then

$$\Sigma\Pi_{eq} = \left(\frac{X_{Ba,aq}}{K_{Ba}\gamma_{Ba}} + \frac{X_{Sr,aq}}{K_{Sr}\gamma_{Sr}}\right)^{-1}. \tag{5.6}$$

In a Lippmann diagram, the solidus and solutus curves are plotted against two superimposed scales (X_{Ba} and $X_{Ba,aq}$). Horizontal tie-lines can be drawn between the solutus and solidus curves, thereby giving the solid-phase–aqueous-phase coexisting compositions for a series of possible thermodynamic equilibrium states. The Lippmann diagram for an ideal $(Ba,Sr)SO_4$ solid solution is shown in figure 6.

It is clear from this figure that an aqueous solution in this system with even a small amount of Ba^{2+} is in equilibrium with almost pure barite, i.e. from the thermodynamic point of view, under near equilibrium conditions, barite should nucleate. However, as we have seen above, the threshold supersaturation for barite is much higher than for celestite, and this leads to interesting phenomena where the interplay of thermodynamics and kinetics controls the resultant product.

(*b*) *Supersaturation in SS–AS systems*

It is necessary to define supersaturation in an SS–AS system because supersaturation controls the relative roles of spiral growth and two-dimensional nucleation across the solid solution. There are a number of different conventions for defining supersaturation in pure one-component systems. In equation (3.1), S is the supersaturation ratio C/C_s. Another way of defining the supersaturation is to use the equation

$\beta = I_{AP}/K_{sp}$, where I_{AP} is the ion activity product in the solution, e.g. $[Ba^{2+}][SO_4^{2-}]$ and K_{sp} is the equilibrium solubility product. The relationship between S and β is $S = \sqrt{\beta}$ (Bosbach *et al.* 1998; Pina *et al.* 2000).

In an SS–AS system, the supersaturation of an aqueous solution cannot be expressed by a unique value, but varies with composition of the solid phase. However, the formulation of a general equation to describe the supersaturation of any given fluid composition with respect to any solid composition, even in a binary SS–AS system, is not a simple task and has not yet been entirely resolved. Currently there exist two alternative formulations. The first (Prieto *et al.* 1993) is based on the concept of stoichiometric saturation (Thorstensen & Plummer 1977), which is a limiting equilibrium state that, in principle, can only be applied to congruent dissolution processes in certain SS–AS systems. In this formulation, the supersaturation β is simply expressed as

$$\beta = \frac{\prod a_i^{\nu_i}}{K_s}, \tag{5.7}$$

where $\prod a_i^{\nu_i}$ is the ionic activity product, ν_i is the stoichiometric number of ion i in the solute formula, and K_s is the solubility product, i.e. the aqueous ion activity product at equilibrium. Applying this expression to the binary solid solution $Ba_xSr_{1-x}SO_4$, and taking into account the Lippmann and Debye–Hückel methods (extensively described in Glynn & Reardon (1990) and in Prieto *et al.* (1989, 1991)), we derive the supersaturation function

$$\beta(x) = \frac{a(Sr^{2+})^{1-x}a(Ba^{2+})^x a(SO_4^{2-})}{(K_{Sr}a_{Sr})^{1-x}(K_{Ba}a_{Ba})^x}, \tag{5.8}$$

where K_{Sr} and K_{Ba} are the solubility products of the end-members, a_{Sr} and a_{Ba} the activities of the $SrSO_4$ and $BaSO_4$ components in the solid solution, respectively and $x = X_{Ba}$ and $1 - x = X_{Sr}$. The shape of the $\beta(x)$ curve depends on the particular values for K_{Sr} and K_{Ba} and on the composition of the given aqueous solution. Further details of the effects of non-ideality in the solid solution may be found in Pina *et al.* (2000).

Recently, an alternative, more general expression for supersaturation has been derived directly from the two conditions of thermodynamic equilibrium for such systems (5.1) (Astilleros *et al.* 2002). If the composition of a given aqueous solution is expressed as an activity fraction $[Ba^{2+}]/[Ba^{2+}]+[Sr^{2+}]$, then one such composition will lie on the solutus line of the Lippmann diagram in equilibrium with a solid whose composition lies on the solidus line and has an activity fraction of $BaSO_4$ in the solid solution of $X^{eq}_{BaSO_4}$. All aqueous solutions with the same activity fraction whose compositions (expressed as $\Sigma\Pi$) lie vertically directly above the solutus line will be supersaturated with respect to this solid composition. To determine this supersaturation with respect to this solid composition, (5.8) (i.e. the $\beta(x)$ function) can be used. This defines the maximum supersaturation of this aqueous solution. To determine the supersaturation relative to any other solid composition, X_{BaSO_4}, two different cases arise. The supersaturation, $\delta(x)$, of the same aqueous solution relative to a solid in which the activity fraction is greater than or equal to the equilibrium value, i.e. $X_{BaSO_4} \geqslant X^{eq}_{BaSO_4}$, is given by

$$\delta_{X_1} = \frac{[Ba^{2+}][SO_4^{2-}]}{X_{Ba}a_{Ba}K_{Ba}}, \tag{5.9 a}$$

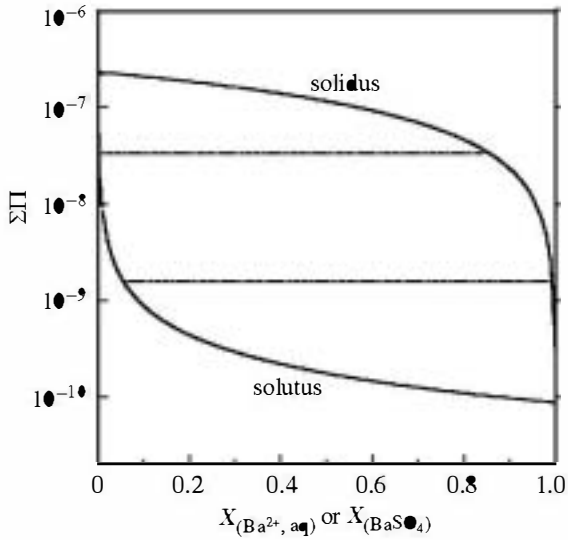

Figure 6. Lippmann diagram for the system $BaSO_4$–$SrSO_4$–H_2O, showing the fluid (solutus) and solid (solidus) compositions at equilibrium. $\Sigma\Pi$ is the total solubility product defined as $[SO_4^{2-}]([Ba^{2+}]+[Sr^{2+}])$.

where $[Ba^{2+}]$ and $[SO_4^{2-}]$ are the activities of the ions in the aqueous solution. The supersaturation, $\delta(x)$, relative to a solid in which the activity fraction is less or equal to the equilibrium value, i.e. for $X_{BaSO_4} \leqslant X^{eq}_{BaSO_4}$,

$$\delta_{X_1} = \frac{[Sr^{2+}][SO_4^{2-}]}{X_{Sr}a_{Sr}K_{Sr}}. \qquad (5.9\,b)$$

Figure 7, curve II shows this supersaturation function, $\delta(x)$, calculated for a fluid in which the [Ba]/[Sr] ratio is 1:2000 (i.e. the activity fraction ~ 0.0005). The maximum supersaturation is for a solid composition with the activity fraction of $BaSO_4 \sim 0.5$. Curve I is the supersaturation, $\beta(x)$, for the same fluid composition calculated using equation (5.7). The two curves correspond to the two alternative functions to calculate supersaturation in SS–AS systems but give the same supersaturation maximum. In the rest of this paper we use the $\delta(x)$ function.

(i) *Macroscopic growth experiments*

The experimental set-up for these growth experiments is similar to that for the pure end-members, except that one reservoir contains both Ba^{2+} and Sr^{2+}. In the same way, the concentrations of all components at the nucleation site is known at the nucleation time, so that given a formulation for the definition of supersaturation, this value as well as its rate of change can be determined.

Crystal-growth experiments using the counter-diffusion of reactants method showed that nucleation is controlled by a complex interplay between the thermodynamics which always favours the nucleation of the least-soluble phase (in this case a Ba-rich phase) and the kinetics which favours nucleation of a more-soluble phase (which has a lower threshold supersaturation for nucleation). Thus at high supersaturation an Sr-rich phase may be the first to nucleate. In the silica hydrogel, transport

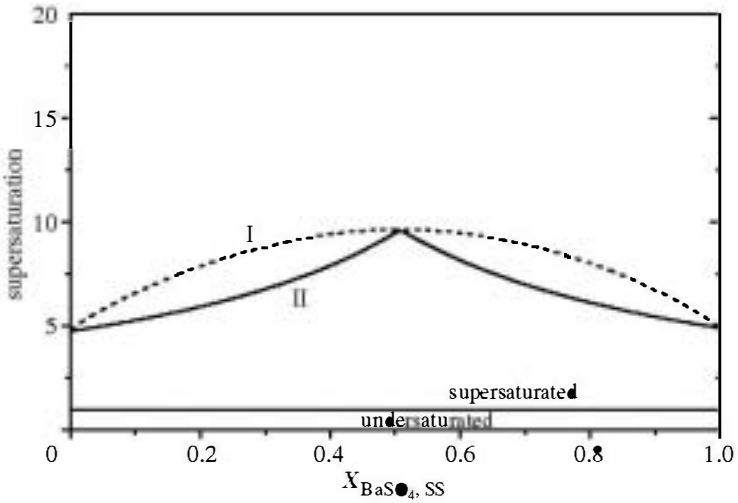

Figure 7. Supersaturation functions for an aqueous solution relative to all possible compositions of the solid solution (Ba,Sr)SO_4. The fluid composition in this case was $[Ba^{2+}] = 1\ \mu mol\ l^{-1}$; $[SO_4^{2-}] = [Sr^{2+}] = 2000\ \mu mol\ l^{-1}$. Curve I is the $\beta(x)$ supersaturation function defined in equation (5.8); curve II is the $\delta(x)$ function defined in equations (5.9 *a*) and (5.9 *b*).

of the reactants is constrained by diffusion, and nucleation of an Sr-rich phase causes local depletion of Sr^{2+}, with enrichment of Ba^{2+} ultimately favouring the growth of a Ba-rich phase. The interplay between growth kinetics and diffusional transport results in periodic instability that causes oscillatory compositional variations in the growing solid-solution crystal (see Putnis *et al.* 1992; Prieto *et al.* 1993, 1997). Oscillatory zoning is a common phenomenon in minerals (Ortoleva *et al.* 1987; Shore & Fowler 1996; Pollok *et al.* 2001) and implies that such chemical self-organization is a regular feature of crystal growth in nature.

(ii) *Crystal-growth experiments of SS–AS systems in a fluid cell in an AFM*

The primary aim of the experiments was to verify the theoretical treatment of the SS–AS system outlined above by *in situ* observation of growth as a function of supersaturation of the aqueous phase. The transitional supersaturation for two-dimensional nucleation was determined as the value of fluid supersaturation at which two-dimensional nucleation could be observed. Some uncertainty in this value arises because time is a factor that increases the probability of nucleation. As noted previously, these transitional values from spiral growth to two-dimensional nucleation of pure $BaSO_4$ on barite (001) occur when $\delta^*_{barite} \sim 7.0$, and for celestite $SrSO_4$ the equivalent value is *ca.* 2.3. To study the nucleation of the (Ba,Sr)SO_4 solid solution, aqueous solutions with different ratios of Ba^{2+}, Sr^{2+} and SO_4^{2-} were passed over barite (001) cleavage surfaces, and nucleation density and incubation time were measured (Pina *et al.* 2000). It was assumed that the transition from spiral growth to two-dimensional nucleation for the solid solution is determined simply as a linear interpolation between the end-members barite and celestite.

Figure 8 shows a typical situation where the supersaturation for a specific aqueous solution composition has been calculated relative to the whole range of solid-solution

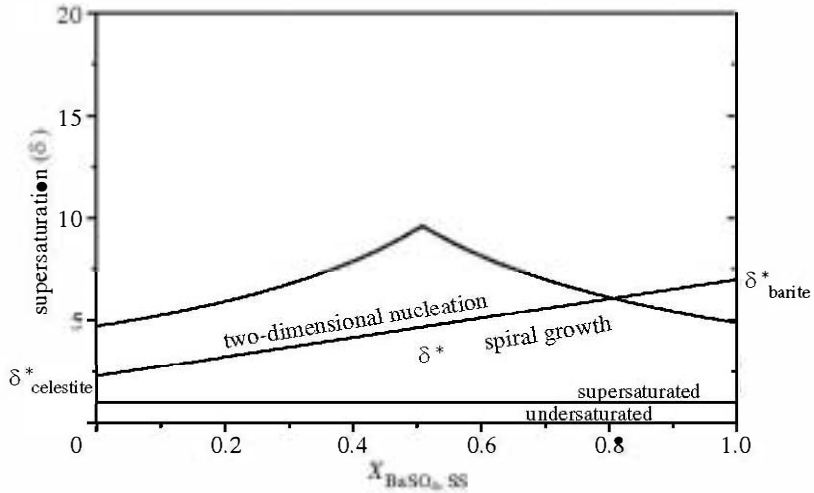

Figure 8. Relationship between the supersaturation function $\delta(x)$ and growth mechanisms. The supersaturation curve corresponds to the same composition as in figure 7. The transitional supersaturation levels for the transition from spiral growth to two-dimensional nucleation are shown as a linear interpolation between the end-member values given by $\delta^*_{\text{celestite}}$ and δ^*_{barite}.

compositions. When the transitional supersaturation line is superimposed the diagram shows those compositions which can only grow by two-dimensional nucleation and those which may grow by spiral growth. Given that the solution is supersaturated with respect to all compositions of the solid solution, this opens the possibility that growth by step advancement and by two-dimensional nucleation may have different chemical compositions on the same substrate.

Figure 9 shows three representative crystallization experiments for which two-dimensional nucleation was observed. For each experiment the supersaturation was calculated using equations (5.8). Figure 9*a* shows the supersaturation distribution for an aqueous solution with composition [Ba] = 1 μmol l^{-1}, [Sr^{2+}] = [SO_4^{2-}] = 3000 μmol l^{-1}. Although this can be virtually considered as an $SrSO_4$ solution with very little added Ba, it is supersaturated with respect to all compositions of the (Ba,Sr)SO_4 solid solution, with a maximum supersaturation (δ = 15) corresponding to a solid-solution composition X_{Ba} = 0.40. Two-dimensional nucleation occurred after an incubation time of *ca.* 350 s. Precipitation is characterized by a high nucleation density (12–20 nuclei μm^{-2}) and by the development of two-dimensional (i.e. one molecular layer thick) islands 3.6 Å high, with ellipsoidal morphologies (figure 9*b*). The islands appear to be distributed over the whole surface and preferentially on the cleavage-step edges.

When a solution with composition [Ba^{2+}] = 1 μmol l^{-1}, [Sr^{2+}] = [SO_4^{2-}] = 2000 μmol l^{-1} is used, the supersaturation levels are reduced (figure 9*c*), but two-dimensional nucleation is again possible for most of the compositions of the (Ba,Sr)SO_4 solid solution ($X_{BaSO_4} < 0.91$). The maximum supersaturation is now δ = 9.5 and relates to a solid composition with molar fraction X_{BaSO_4} = 0.49, and this has an obvious effect on the nucleation parameters. The nucleation density decreases (N_i = 3–4 nuclei μm^{-2}) and the incubation time increases (t_i = 660 s). Again, nucleation does not occur homogeneously on the initial barite substrate,

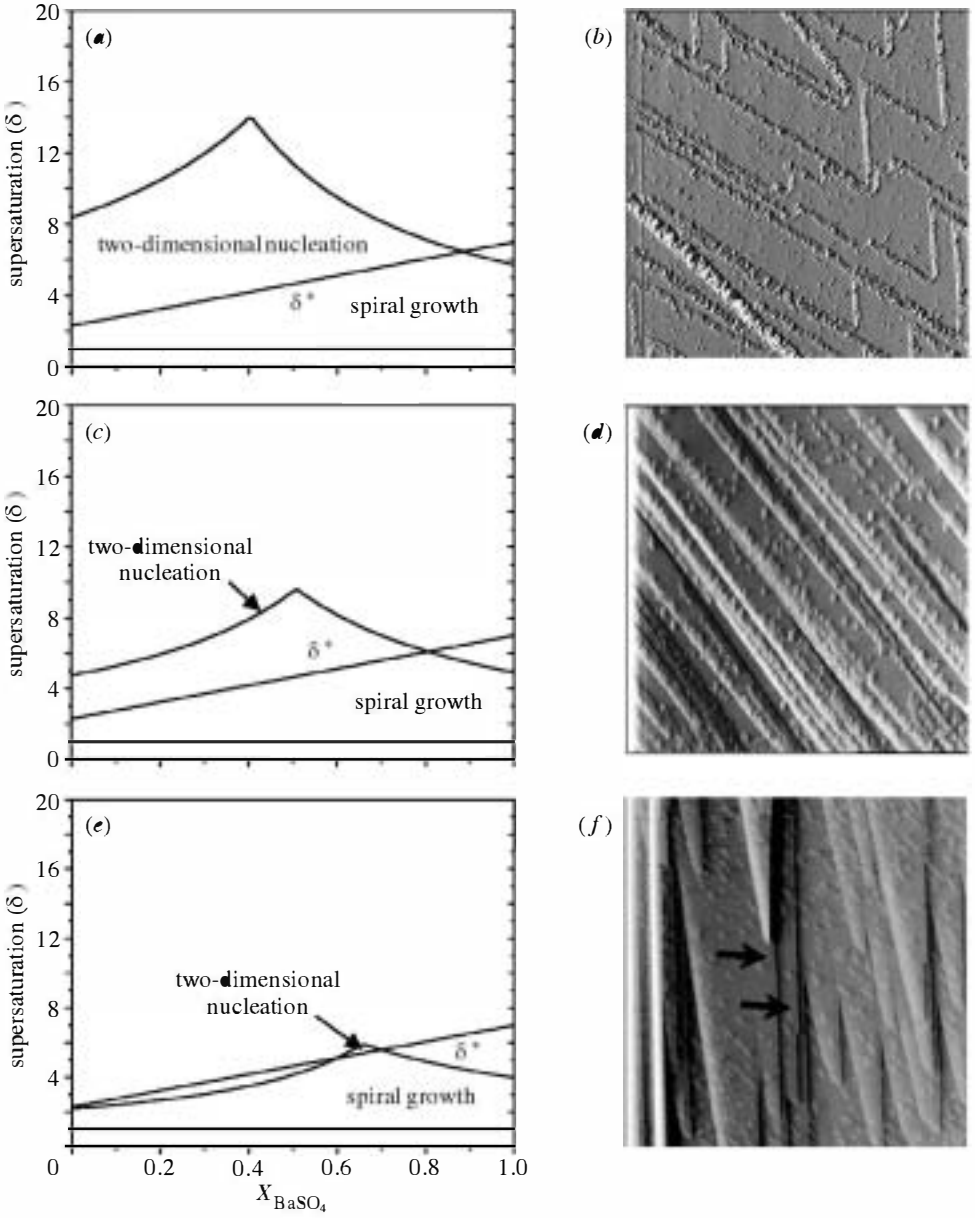

Figure 9. Supersaturation–solid composition diagrams and AFM images of the barite (001)-face during growth. The scan area is 15 μm × 15 μm in all cases. (*a*), (*c*) and (*e*) The supersaturation functions for three different solutions containing Ba, Sr and SO_4 ions, in a sequence of decreasing supersaturation; (*b*), (*d*) and (*f*) are the corresponding experimental images. For further experimental details see text.

but nuclei are distributed preferentially along the step edges (figure 9*d*). Finally, figure 9*e* shows the diagram corresponding to a solution with $[Ba^{2+}] = 1\ \mu mol\ l^{-1}$, $[Sr^{2+}] = [SO_4^{2-}] = 1100\ \mu mol\ l^{-1}$. The maximum supersaturation ($\delta = 6.0$) occurs for

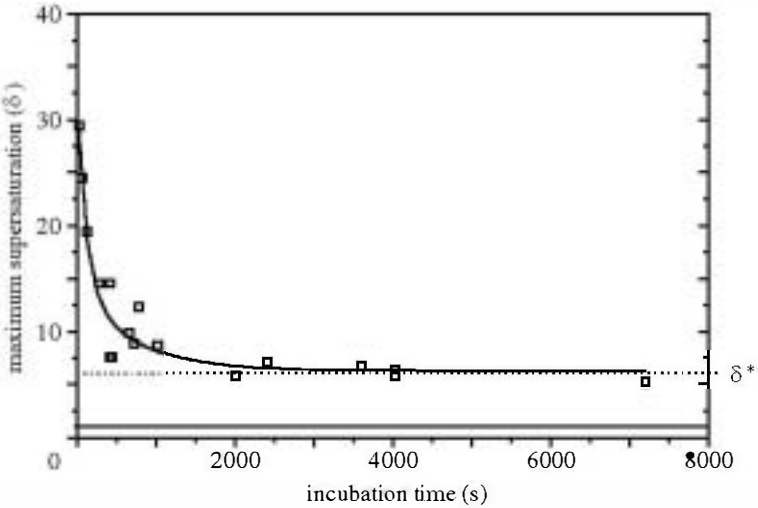

Figure 10. Maximum supersaturation versus incubation time for two-dimensional nucleation in the system $BaSO_4$–$SrSO_4$–H_2O. The data are obtained from experiments such as shown in figure 9.

the solid composition $X_{BaSO_4} = 0.65$, and the supersaturation curve lies only just above the $\delta^*_{celestite}$–δ^*_{barite} line. In this case, two-dimensional nucleation can only occur for solid compositions with molar fractions $0.03 < X_{BaSO_4} < 0.71$. Nucleation on a barite surface in contact with this solution was detected only after a long incubation time, $t_i = 4021$ s. The nucleation density is, however, quite similar to that observed in the previous case ($N_i = 2$–2.5 nuclei μm^{-2}) (figure 9*f*). These islands again form preferentially on the initial cleavage steps. In this image the advance of these initial (arrowed) cleavage steps can also be observed.

For dilute Ba^{2+}–Sr^{2+}–SO_4^{2-} solutions, whose supersaturation curve lies below the δ^* line, two-dimensional nucleation is theoretically not possible, and the only possible growth mechanism is the advance of cleavage steps and spiral growth. The existence of such a transitional supersaturation line is reflected in the increase in the incubation time when the solutions used are progressively less concentrated. Figure 10 shows the relationship between supersaturation and incubation time. The incubation time (i.e. the time elapsed between injection of the solution and observation of the first nuclei on the surface) was measured for a range of solution compositions with decreasing supersaturation relative to the (Ba,Sr)SO_4 solid solution. As the supersaturation is reduced, the incubation time exponentially increases. The exponential dependence of the incubation time on the maximum supersaturation (which corresponds in all cases to intermediate compositions and constitutes an indicator of the decrease in the supersaturation values for the complete solid solution) shows that below $\delta \approx 6$, corresponding to solutions with sulphate and strontium concentrations below 1000 μM (and with $[Ba^{2+}] = 1\,\mu M$), the incubation time is infinity. This indicates that the original assumption of a linear interpolation of δ^* between the two end-members is essentially correct, and it demonstrates that the variation of solubility with solid-solution composition is the main factor controlling the change in growth mechanisms.

6. Conclusions

There is a systematic relationship between the threshold supersaturation for nucleation and the supersaturation rate for a wide range of systems.

In situ AFM studies can identify the growth mechanisms as a function of supersaturation. In certain crystal symmetries where anisotropy in growth rates is dependent on crystallographic orientation, spiral growth may not be viable and may require two-dimensional nucleation and growth to be taking place at the same time.

In SS–AS systems at high supersaturation there is often a conflict between the thermodynamics and kinetics of nucleation and growth. One possible result of this is oscillatory compositional zoning.

The supersaturation of fluids relative to solid solutions has been defined and compared with experimental observation of crystal growth in SS–AS systems. Direct observations of nucleation and incubation times are consistent with the theory presented.

This work is supported by grants from the Deutsche Forschungsgemeinschaft, the Science and Technology Commission of Spain, the Marie Curie Fellowship Scheme of the EU and the EU Network 'Quantifying dissolution and precipitation of solid solutions in natural and industrial processes' (Contract no. HPRN-CT-2000-00058).

References

Astilleros, J. M., Pina, C. M., Fernández-Díaz, L. & Putnis, A. 2002 Supersaturation functions in binary solid solution–aqueous solution systems. *Geochim. Cosmochim. Acta.* (In the press.)

Becker, U., Fernández-Gonzáles, A., Prieto, M., Harrison, R. & Putnis, A. 2000 Direct calculation of the thermodynamic properties of the barite–celestite solid solution from molecular principles. *Phys. Chem. Miner.* **27**, 291–300.

Blount, C. W. 1977 Barite solubilities and thermodynamic quantities up to 300 °C and 1400 bars. *American Mineralogist* **62**, 942–957.

Bosbach, D., Hall, C. & Putnis, A. 1998 Mineral precipitation and dissolution in aqueous solution: in-situ microscopic observations on barite (001) with atomic force microscopy. *Chem. Geol.* **151**, 143–160.

Burton, W. K., Cabrera, N. & Frank, F. C. 1951 The growth of crystals and the equilibrium structure of their surfaces. *Phil. Trans. R. Soc. Lond.* A **243**, 299–358.

Chernov, A. A. 1984 *Modern crystallography III: crystal growth*, p. 517. Springer.

Glynn, P. D. & Reardon, E. J. 1990 Solid-solution aqueous-solution equilibria: thermodynamic theory and representation. *Am. J. Sci.* **290**, 164–201.

Henisch, H. K. 1989 *Crystals in gels and Liesegang rings.* Cambridge University Press.

Khamskii, E. V. 1969 *Crystallization from solutions.* New York: Consultants Bureau, Plenum.

Lippmann, F. 1980 Phase diagrams depicting the aqueous solubility of mineral systems. *Neues Jahrbuch Mineralogische Abhandlungen* **139**, 1–25.

Lippmann, F. 1982 Stable and metastable solubility diagrams for the system $CaCO_3$–$MgCO_3$–H_2O at ordinary temperature. *Bull. Mineral.* **105**, 273–279.

Mullin, J. W. 1993 *Crystallization*, 3nd edn. Oxford: Butterworth.

Nielsen, A. E. 1964 *The kinetics of precipitation.* Oxford: Pergamon.

Nielsen, A. E. 1984 Electrolyte crystal-growth mechanisms. *J. Cryst. Growth* **67**, 289–310.

Nielsen, A. E. & Toft, J. M. 1984 Electrolyte crystal-growth kinetics. *J. Cryst. Growth* **67**, 278–288.

Nývlt, J. 1968 Kinetics of nucleation in solutions. *J. Cryst. Growth* **3**, 377–383.

Ohara, M. & Reid, R. C. 1973 *Modeling crystal-growth rates from solution.* Englewood Cliffs, NJ: Prentice-Hall.

Orteleva, P., Merino, E., Moore, C. & Chadam, J. 1987 Geochemical self-organization. I. Reaction-transport feedbacks and modeling approach. *Am. J. Sci.* **287**, 979–1007.

Pina, C. M., Becker, U., Risthaus, P., Bosbach, D. & Putnis, A. 1998*a* Molecular-scale mechanisms of crystal growth in barite. *Nature* **395**, 483–486.

Pina, C. M., Bosbach, D., Prieto, M. & Putnis, A. 1998*b* Microtopography of the barite (001) face during growth: AFM observations and PBC theory. *J. Cryst. Growth* **187**, 119–125.

Pina, C. M., Enders, M. & Putnis, A. 2000 The composition of solid solutions crystallising from aqueous solutions: the influence of supersaturation and growth mechanisms. *Chem. Geol.* **168**, 195–210.

Pollok, K., Jamtveit, B. & Putnis, A. 2001 Analytical transmission electron microscopy of oscillatory zoned grandite garnets. *Contrib. Mineral. Petrol.* **141**, 358–366.

Prieto, M., Viedma, C., López-Acevedo, V., Martín-Vivaldi, J. L. & López-Andrés, S. 1989 Mass transfer and supersaturation in crystal growth in gels. *J. Cryst. Growth* **92**, 61–68.

Prieto, M., Putnis, A. & Fernández-Díaz, L. 1990 Factors controlling the kinetics of crystallization: supersaturation evolution in a porous medium. Application to barite crystallization. *Geol. Mag.* **127**, 485–495.

Prieto, M., Fernández-Díaz, L. & López-Andrés, S. 1991 Spatial and evolutionary aspects of nucleation in diffusing–reacting systems. *J. Cryst. Growth* **108**, 770–778.

Prieto, M., Putnis, A. & Fernández-Díaz, L. 1993 Crystallization of solid solution from aqueous solutions in a porous medium: zoning in (Ba,Sr)SO_4. *Geol. Mag.* **130**, 289–299.

Prieto, M., Fernández-Díaz, L. & López-Andrés, S. 1994 Metastability in diffusing–reacting systems. *J. Cryst. Growth* **108**, 770–778.

Prieto, M., Fernández-González, A., Putnis, A. & Fernández-Díaz, L. 1997 Nucleation, growth and zoning phenomena in crystallizing (Ba,Sr)CO_3, Ba(SO_4, CrO_4), (Ba,Sr)SO_4, and (Cd, Ca)CO_3 solid solutions from aqueous solutions. *Geochim. Cosmochim. Acta* **61**, 3383–3397.

Putnis, A., Fernández-Díaz, L. & Prieto, M. 1992 Experimentally produced oscillatory zoning in the (Ba,Sr)SO_4 solid solution. *Nature* **358**, 743–745.

Putnis, A., Prieto, M. & Fernández-Díaz, L. 1995 Fluid supersaturation and crystallisation in porous media. *Geol. Mag.* **132**, 1–13.

Reardon, E. J. & Armstrong, D. K. 1987 Celestite ($SrSO_4$(s)) solubility in water, sea water and NaCl solution. *Geochim. Cosmochim. Acta* **51**, 63–72.

Risthaus, P., Bosbach, D., Becker, U. & Putnis, A. 2001 Barite scale formation and dissolution at high ionic strength studied with atomic force microscopy. *Colloids Surf.* A **191–193**, 201–214.

Sarig, S. 1993 Fundamentals of crystal growth. In *Handbook of crystal growth* (ed. D. T. J. Hurle), vol. 2B. Amsterdam: Elsevier.

Shore, M. & Fowler, A. D. 1996 Oscillatory zoning in minerals: a common phenomenon. *Can. Mineralogist* **34**, 1111–1126.

Söhnel, O. 1982 Electrolyte crystal-aqueous solution interfacial tensions from crystallisation data. *J. Cryst. Growth* **57**, 101–108.

Sunagawa, I. 1984 Growth of crystal in nature. In *Materials science of the Earth's interior* (ed. I. Sunagawa). Tokyo: Terra Scientific.

Sunagawa, I. 1987 *Morphology of crystals. Part A.* Tokyo: Terra Scientific.

Sunagawa, I. 1993 Investigations of crystal growth in Earth and planetary science. In *Handbook of crystal growth* (ed. D. T. J. Hurle), vol. 2B. Elsevier.

Thorstensen, D. C. & Plummer, L. N. 1977 Equilibrium criteria for two-component solids reacting with fixed composition in an aqueous-phase. Example: the magnesian calcites. *Am. J. Sci.* **277**, 1203–1223.

Walton, A. G. 1967 *The formation of precipitates.* Wiley Interscience.

Walton, A. G. 1969 Nucleation in liquids and solutions. In *Nucleation* (ed. A. C. Zettlemoyer), pp. 225–307. New York: Marcel Dekker.

K. F. KELTON (*Department of Physics, Washington University, St Louis, MO, USA*). The measured inaction times seem to scale in the correct way with supersaturation based on, say, the Koskchiev expression. Did you try to fit your data to this expression?

A. PUTNIS. No, we have not tried that, but thank you for the suggestion.